On the Importance of the Stokes–Brinkman Equations for Computing Effective Permeability in Carbonate Karst Reservoirs

Marcin Krotkiewski[1,*], Ingeborg S. Ligaarden[2], Knut–Andreas Lie[2,3], and Daniel W. Schmid[1]

[1] *Physics of Geological Processes, University of Oslo, P.O. Box 1048 Blindern, NO–0316 Oslo, Norway*
[2] *SINTEF ICT, Department of Applied Mathematics, P.O. Box 124 Blindern, NO-0314 Oslo, Norway*
[3] *Center of Mathematics for Applications, University of Oslo, P.O. Box 1053 Blindern, NO–0316 Oslo, Norway*

Abstract. Cavities and fractures significantly affect the flow paths in carbonate reservoirs and should be accurately accounted for in numerical models. Herein, we consider the problem of computing the effective permeability of rock samples based on high-resolution 3D CT scans containing millions of voxels. We use the Stokes-Brinkman equations in the entire domain, covering regions of free flow governed by the Stokes equations, porous Darcy flow, and transitions between them. The presence of different length scales and large (ten orders of magnitude) contrasts in permeability leads to highly ill-conditioned linear systems of equations, which are difficult to solve. To obtain a problem that is computationally tractable, we first analyze the relative importance of the Stokes and Darcy terms for a set of idealized 2D models. We find that, in terms of effective permeability, the Stokes-Brinkman equations are only applicable for a special parameter set where the effective free-flow permeability is less than four orders of magnitude different from the matrix permeability. All other cases can be accurately modeled with either the Stokes or the Darcy end-member flows, depending on if there do or do not exist percolating free-flow regions. The insights obtained are used to perform a direct computation of the effective permeability of a rock sample model with more than 8 million cells.

AMS subject classifications: 35B27, 35Q30, 6S05

Key words: Upscaling, Stokes equation, Brinkman equation, porous media

*Corresponding author. *Email addresses:* marcink@fys.uio.no (M. Krotkiewski), Ingeborg.Ligaarden@sintef.no (I. S. Ligaarden), Knut-Andreas.Lie@sintef.no (K.-A. Lie), schmid@fys.uio.no (D. W. Schmid)

1 Introduction

Numerical simulation of flow and transport in carbonate reservoirs is a challenging problem. Carbonate reservoirs are composed of porous material, which contains cavities and fractures on multiple scales and throughout the entire rock formation. The presence of these, often relatively large void spaces affects the flow paths in the medium and should be accurately accounted for in the numerical model.

On the microscale, flow through individual pores and pore throats typically occurs at relatively low Reynold's numbers and can hence be described by the incompressible Stokes equation. On the macroscale, one can for obvious reasons not resolve the flow through individual pores and pore throats, and the flow is instead modelled using Darcy's law (and mass conservation). This macroscale description requires a set of effective petrophysical parameters—porosity and permeability—that describe the average ability of a rock to store and transport fluids, respectively. Permeability is characteristic for a given material and scale, and can be obtained from laboratory experiments, analytical upscaling formulas, or by upscaling flow simulations of rock models on a smaller scale. Herein, we consider the problem of computing such effective permeabilities for a small-scale representative elementary volume (REV) consisting of a high-resolution 3D rock sample obtained from a CT scan. The effective permeability will then be used to populate geological models on a larger scale with correct petrophysical paramters, which may then again be upscaled to enable flow simulations on the scale of the reservoir. This is typically performed using a coarse model with low numerical resolution. In this approach, due to the nature of the upscaling, all the information about the fine-scale flow structure, like fluid-front propagation and stagnant zones (important e.g., for estimating the residual fluid saturation) is lost. Other methods, such as the multiscale approach [9], aim at solving flow equations on a coarse model, while still being able to restore the fine-scale flow structure.

The standard approach to compute effective permeabilities is to solve a single-phase flow problem with a unit pressure drop applied in each axial directions of the rock sample. If the rock sample consists of only porous material, the flow inside the REV is described using the Darcy equations, as on the macro-scale. On the other hand, if the REV also contains void spaces, in which free flow may occur, one may need a more sophisticated model. To this end, there are two main approaches. The flow can either be described by a system consisting of Darcy's law for the porous material and the Stokes equation for the voids, coupled with the Beavers–Joseph–Saffman conditions on the boundaries between the porous and void volumes, see [1–4]. Alternatively, one can use the Stokes–Brinkman equations, which give a seamless transition between the Stokes and Darcy equations, see [5, 14, 15].

Herein, we assume that the Stokes–Brinkman model is best suited to describe the fine-scale flow. Irrespective of this choice, solving the flow problem numerically is a challenging task. High-resolution models obtained from CT scans typically contain millions of voxels: the particular model we consider consists of more than eight million cells. Solv-

ing the Darcy–Stokes and the Stokes–Brinkman equations requires higher-order methods [2, 11, 15, 18], which in 3D leads to discrete systems with 100 million to a billion degrees of freedom. It is well-known that for high-resolution 3D discretizations, the cost of solving linear systems of equations using direct solvers is prohibitive because of the superlinear scaling of the work and storage requirements with the system size. Instead, well parallelizable iterative solvers, e.g., conjugate gradients, or MINRES are often used. In this case, the number of iterations required to converge to a satisfactory solution depends on the condition number of the system matrix. Dealing with different length scales and large (ten orders of magnitude) contrasts in permeability leads to highly ill-conditioned linear systems of equations, see e.g., [2]. Consequently, solving either the Darcy–Stokes or the Stokes–Brinkman equations for our particular model is too expensive even on a high-performance supercomputer.

In the following, we take an alternative approach and identify simplifications that render the fine-scale flow problem computationally tractable. We consider a set of idealized 2D models and determine the parameter ranges for which the full Stokes–Brinkman equations are necessary, and for which the effective permeability can be computed by either Darcy or Stokes solvers alone. The insights obtained from the synthetic models are then used to compute the effective permeability of the presented rock sample model in 2D and 3D.

2 Model of a Rock Sample

As an example of a typical rock model, we will in the following use a specific model that was obtained from a CT scan of a $13 \times 13 \times 21$ cm carbonate rock sample [19]. The resolution of the CT scan was roughly $0.5 \times 0.5 \times 1.5$ mm, giving a model that consists of $240 \times 240 \times 144$ regular voxels. The porosity of the rock sample has been obtained on the assumptions that the host rock is pure calcite with a constant grain density, that the air density is zero, and that the relationship between the CT image values and the density is linear. Void spaces (vugs) have been identified as regions with low or zero density. The permeability of the matrix has been computed based on an upscaling formula by Jennings and Lucia [10]. Minimum permeability in the matrix is $10^{-4}mD$, maximum permeability is $10^{3}mD$.

The model is visualized in Figure 1, which shows the permeability. The red zones are void spaces (vugs), where we expect free flow. From the visualization, and in particular from the 2D slice, one may get the impression that the vugs are not connecting one side of the model to the other, while in fact they do. Figure 2 shows a volume rendering of the three-dimensional structure of the void spaces inside the rock sample (in gray) with the borders between void space and porous material plotted in a yellowish color. To simplify the visualization, we have filtered out all isolated void spaces that are completely surrounded by the porous matrix, so that the figure only shows the vugs that are connected to the top and bottom of the sample.

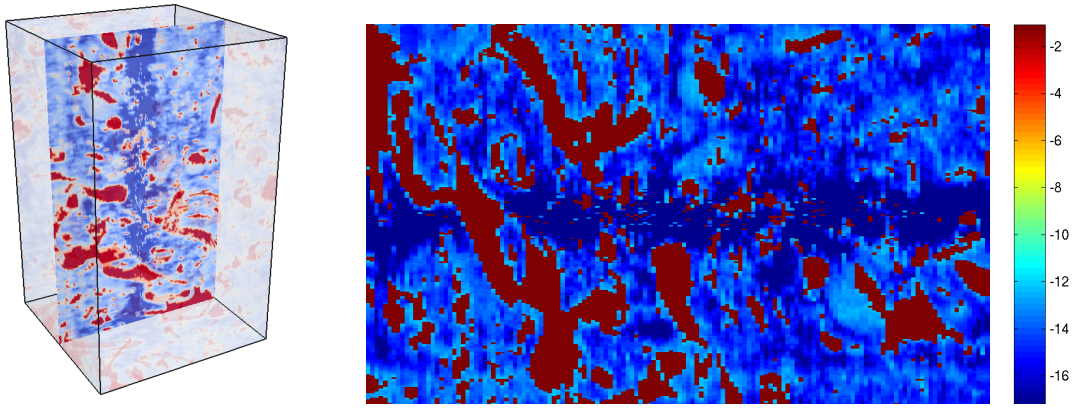

Figure 1: 3D permeability model of a rock sample with physical dimensions $13 \times 13 \times 21$ cm. The permeability is given on a regular grid with $240 \times 240 \times 144$ cells. The left plot shows the 3D permeability with a 2D cut through the domain. Here, red color denotes the void spaces (vugs). The right plot shows the 2D cut in more detail, with the permeability plotted on a logarithmic scale.

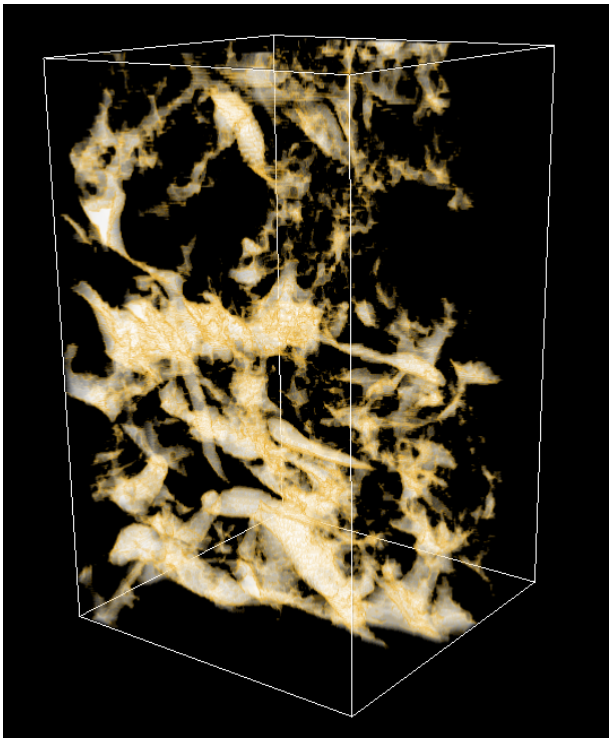

Figure 2: Volume rendering of the 3D channels connecting the top and bottom of the model. The void volumes are shown in gray, and the void borders are marked with a yellowish color.

To compute the effective permeability of the sample one could directly solve the Stokes–Brinkman equations and include the entire porous matrix and the free-flow regions in the computations. However, as explained before, the resulting linear system of equations is too large to solve using direct solvers, and too ill-conditioned to solve using iterative methods.

From a computational point of view, it would be advantageous if the model did not contain through-going void spaces. Then, we could use a two-step upscaling procedure to compute effective permeabilities for the sample. That is, we could partition the model into a set of non-overlaping and smaller REVs, and solve local flow problems to compute effective permeabilities of each of them. The obtained permeabilities could then be used on the intermediate scale to approximate the flow through the original model using significantly fewer degrees of freedom. However, the results obtained in this manner have been unsatisfactory: after upscaling to a regular intermediate grid, the void spaces have been averaged out over the intermediate REVs, and the connection between the sides of the model through the void space has been lost.

A simple, but not necessarily correct, alternative to flow-based upscaling is to directly compute an upscaled permeability by averaging of the fine-scale permeability. For our particular problem, the validity of this approach rests on the major assumption that the flow in the vugs can be described by the Darcy equation and that we can assign an appropriate permeability to the vugs. Because of the complicated geometry of the vug network of the 3D model, it is far from trivial to compute a proper permeability value for the vugs without experimental data and/or extensive tuning of parameters. The 1/3-power averaging method [16] was applied to the 3D model in [19], showing that the local power averaging fails to preserve the fine-scale connectivity of the vugs, hence underestimating the effective permeability.

As we will see later, the connection through void space is the most important factor for determining the effective permeability of this particular sample, and will be the key to developing an effective strategy for solving flow problems inside the REV. However, before we give more details in this direction, we will in the next section present the Stokes–Brinkman equations and discuss numerical strategies for solving them.

3 The Stokes–Brinkman Equations

The Stokes–Brinkman equations for single-phase, incompressible fluid flow in a mixed free-flow and porous medium proposed by Brinkman [5] are

$$\begin{aligned} \nabla p = -\mu \mathbf{K}^{-1}\vec{v} + \nabla \cdot \mu^*(\nabla\vec{v} + \nabla\vec{v}^T) \\ \nabla \cdot \vec{v} = 0 \end{aligned} \tag{3.1}$$

Here, p is the fluid pressure, $\vec{v}$ is fluid velocity, $\mathbf{K}$ is the permeability tensor, μ is the fluid viscosity, and μ^* is the so-called *effective viscosity* of the fluid. By choosing the param-

eters appropriately, one can study the two end-member cases: for infinite permeability we obtain Stokes flow, for $\mu^* = 0$ we have the Darcy flow.

In the literature, the Stokes term in (3.1) is frequently written in the Laplace form $(\mu^* \nabla^2 \vec{v})$. It is also often assumed that $\mu = \mu^*$. However, it is generally agreed that the value of μ^* depends on the properties of the porous medium. It has been shown that the effective viscosity can be either smaller, or greater than the fluid viscosity μ. The effect is commonly attributed to tortuosity and porosity. For an in-depth discussion and a list of references the reader is referred to [13].

3.1 Numerical Solution in 2D

To solve (3.1), we use a mixed finite-element formulation with distinct degrees of freedom defined for velocity and pressure variables. The elements are the seven-node Crouzeix–Raviart triangle with quadratic velocity shape functions enhanced by a cubic bubble function, and a nine-node quad with quadratic velocity field. The pressure field is discontinuous, with linear shape functions. These elements have a number of advantages over other elements used for the Stokes and Stokes–Brinkman equations, e.g., the Taylor–Hood element used in [9,15]. The incompressibility constraint from (3.1) is implemented using the penalty method, i.e., the right-hand side of the divergence equation is set to p/λ. Then, incompressibility is assured by choosing a relatively small penalty parameter λ and using the Powell and Hestenes iterations. Since the pressure is discontinuous, it is possible to eliminate the pressure degrees of freedom on a per-element basis (static condensation). The resulting global system of equations has fewer degrees of freedom, and is symmetric and positive-definite, as opposed to the original system (3.1). It is factorized once using Cholesky factorization, and the factor is reused during the Powell and Hestenes iterations. Typically, the incompressible solution is obtained after less than ten iterations.

The solver is implemented in the modified[†] MILAMIN package [6], which is an efficient Matlab finite-element solver capable of setting up, solving, and post-processing two-dimensional problems with one million unknowns in one minute on a standard desktop PC. The code works for both unstructured adaptive, and structured meshes, for triangular and quad elements. The ability to deal with such resolutions in a matter of seconds is crucial to resolve the complex geometries found in geological systems. Moreover, MILAMIN has been designed to efficiently deal with large material property ratios, which is a must when modeling heterogeneous rocks and fluids. The code has been optimized to the point, where the only bottleneck is the linear solver. For the solution of the linear system of equations we use CHOLMOD [7]. For a more thorough description of the numerical method and the implementation, the reader is referred to [6].

[†]Modifying MILAMIN to deal with the Stokes–Brinkman equations requires adding the Darcy term, which is equivalent to updating the element stiffness matrix by the element mass matrix scaled by the permeability and fluid viscosity.

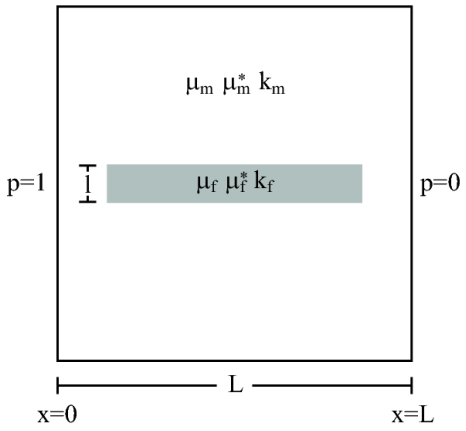

Figure 3: Simple sketch of the idealized model and the parameters: L denotes the domain height and width, ℓ is the crack height. Pressure is set to 1 at $x=0$ and to 0 at $x=L$. For simplicity, fluid viscosity and effective viscosity in the crack and the matrix are the same.

3.2 Numerical Solution in 3D

For three-dimensional models, direct solvers are too expensive [6]. The scaling of both memory and computational requirements is non-linear with respect to the size of the linear system of equations. A common approach is to use preconditioned iterative methods. Their advantage is the linear workspace scaling, and good parallel performance.

Hence, the solution strategy for three-dimensional systems is different than in the 2D case. We do not use the penalty method, but rather include the pressure degrees of freedom in the system matrix. The resulting system of equations is symmetric and indefinite (zeros on the main diagonal). To solve it we use the MINRES solver [8], preconditioned with a block preconditioner. The implementation is scalable on over five thousand CPU cores, and reaches performance of 5 TeraFLOPS [12].

4 Parameter Study

In this section, we analyze the importance of using the Stokes–Brinkman equations, as opposed to either Darcy or Stokes equations, to compute an accurate effective permeability of the rock sample presented in Section 2. The numerically upscaled effective permeability can then be used in coarse-scale flow computations, as described by e.g., [3, 15]. We will not analyze the quality of the upscaling itself (i.e., how well coarse-grid calculations approximate the fine-grid results), but rather compare different methods of computing the effective permeability. Our analysis relies entirely on the assumption that all we need to capture on the coarse scale is the effective permeability. If one also needs to resolve the effects of subscale variations (e.g., on the velocity field), a better approach would be to use a multiscale method [9, 18].

To analyze the importance of Darcy versus Stokes terms in the Stokes–Brinkman

model, we will use a set of idealized 2D models (Figure 3), that will be discretized using an unstructured adaptive triangular mesh generated with *Triangle* [17]. Three scenarios are analyzed: a homogeneous model (no crack), a crack surrounded by the matrix (i.e., not touching the left and right boundaries), and a through-going (percolating) crack that touches both boundaries. The insights obtained from these synthetic experiments will then be used in Section 5 to obtain the effective permeability of the rock sample presented in Section 2.

For all three cases, the fluid flow is driven by a horizontal pressure difference Δp. With the Darcy equations, this corresponds to setting $p = \Delta p$ at $x = 0$ and $p = 0$ at $x = L$. In the Stokes and Stokes–Brinkman equations, the fluid pressure cannot be constrained directly. Instead, we obtain an ambient pressure gradient by loading the system with a normal force and constraining the tangential velocity component to zero.

The boundary conditions at $y = 0$ and $y = 1$ must be considered carefully. For Darcy flow, the natural choice is to use either periodic or free-slip boundary conditions ($v_y = 0$, v_x is free). For Stokes flow, additional constraints are required for the velocities in the x-direction in order to avoid translation. Therefore, to be able to study the transition zone between the Darcy and Stokes regimes, we will in all the cases (Darcy and Stokes) use no-slip boundary conditions (v_x=0, v_y=0). For Stokes flow, this setup corresponds to 2D Poiseuille flow in a channel, for which the effective permeability is given by:

$$k_S = \frac{L^2}{12} \tag{4.1}$$

To simplify the discussion, we will rescale the flow equations. The extent of the domain is equal in both spatial directions, and hence we choose the domain width L as the characteristic length scale. To reduce the number of variables, the effective viscosity μ^* and the fluid viscosity μ are set equal and scaled by μ. Choosing Δp as the characteristic pressure unit yields the following dimensionless parameters:

$$\hat{\ell} = \frac{\ell}{L}, \qquad \hat{\mathbf{K}} = \frac{\mathbf{K}}{L^2}, \qquad \hat{\mu}^* = \frac{\mu^*}{\mu}, \qquad \hat{\vec{v}} = \frac{\vec{v}\mu}{L\Delta p}.$$

To simplify the notation, we will henceforth assume that all the parameters are dimensionless and drop the hat symbol, writing ℓ rather than $\hat{\ell}$, etc. When using dimensional parameters, this will be stated clearly.

For all three cases considered, we compute the specific discharge through the boundary at $x = L$ as

$$q = \frac{1}{L}\int_0^L v_x dy.$$

Then, the effective permeability of the domain can be obtained from Darcy's law over the REV

$$k_{\text{eff}} = -\frac{q\mu L}{\Delta p}. \tag{4.2}$$

Numerical Accuracy

As noted above, we are forced to use no-slip boundaries to be able to investigate the entire range of flows. In the case of Darcy flow, this is inconsistent and introduces a numerical error in the velocity field close to the model boundaries. The error depends on the mesh resolution. Similar problems will be observed for a high-permeability channel surrounded by a low-permeability matrix in any Darcy solver that uses a discretization with a continuous velocity field (e.g., Taylor–Hood and Crouzeix–Raviart elements). Velocities in the low-permeable areas will be close to zero, effectively introducing the problem described above. To obtain a correct solution, the Darcy equations should be discretized using elements with a continuous normal velocity component and a discontinuous tangential velocity component, e.g., the lowest-order Raviart–Thomas elements. However, these elements are not suitable for the Stokes end-member case. For the Stokes–Brinkman equations, an interesting formulation was recently presented by Willems [18], who extended a discontinuous Galerin method for the Stokes equations to the Stokes–Brinkman case by using lowest order Brezzi–Douglas–Marini mixed finite-element spaces.

In the three cases studied in this section, the mesh-dependent error error is localized at the boundary. We therefore conducted a mesh-convergence study to determine the mesh resolution that is sufficient to guarantee that the error between the computed and the expected effective permeability in the Darcy case is less than 0.2%. Thus, the obtained results are accurate for both Darcy and Stokes regimes.

4.1 Homogeneous Domain

A homogeneous and isotropic domain is first analyzed. This model is an analogue of a channel filled with an incompressible fluid. When the channel only contains the fluid, the flow is described by the Stokes equations. When a rigid, non-moving matrix is present, the flow meets a certain resistance from the structure. In case we know the exact shape of the obstacles, this can be modeled by solving the Stokes equations and directly resolving the skeleton. In the Stokes–Brinkman approach, this effect is accounted for by the presence of the (upscaled, or averaged) Darcy term. The parameter describing the strength of this effect is the matrix permeability k. For large permeabilities, the flow will be Stokes-like. For small permeabilities, only the Darcy term will be important.

Using the Stokes–Brinkman equations we compute the effective permeability k_{eff} in both end-member cases of Darcy flow and Stokes flow, as well as in the transition zone between the end-member cases to analyze the influence of the matrix permeability on the regime of the flow.

Figure 4 shows the computed effective permeability k_{eff} normalized by the matrix permeability k_m, as a function of the matrix permeability. In the Darcy regime, we expect $k_{\text{eff}} = k_m$, hence the plot saturates at one. In the Stokes regime $k_{\text{eff}}/k_m = L^2/(12 \cdot k_m)$, which approaches zero for large matrix permeabilities. In the transitional regime, the contribution of both the Darcy and the Stokes terms are on the same order. Importantly, for $k_m \leq 10^{-4}$ the Stokes effects no longer play any role, and the problem is essentially of

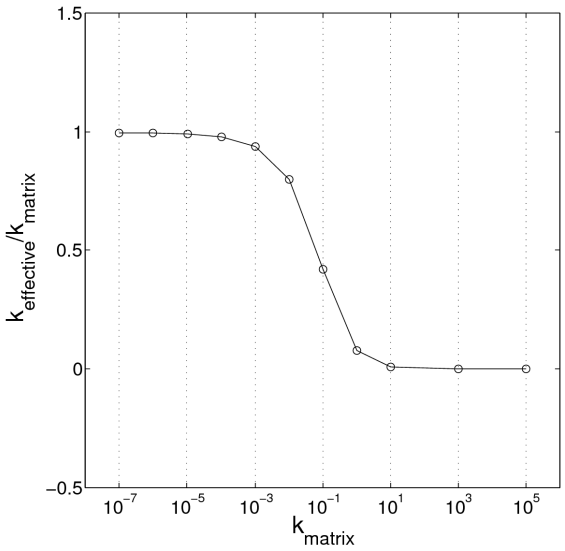

Figure 4: Stokes–Brinkman equations solved in a homogeneous, isotropic domain. The plot shows the computed effective permeability k_{eff} normalized by the matrix permeability k_m. For small matrix permeabilities ($k_m \leq 10^{-4}$) the problem is essentially of Darcy type. For large permeabilities the Stokes term is dominant.

Darcy type. Consider a geological system with a channel of diameter L containing fill-in material with permeability k. Then, the Stokes effects in the channel can be ignored if $k/L^2 \leq 10^{-4}$.

4.2 Confined Fracture

In the next case, we consider a fracture entirely surrounded by the matrix. The fracture

is modeled as a free-flow large aspect ratio rectangle, i.e., the fracture permeability is set to $k_f = \infty$, which means that the Darcy term in the Stokes–Brinkman equations is zero. In the matrix, the Stokes–Brinkman equations are solved.

Figure 5 shows the computed effective permeability normalized by the matrix permeability, as a function of the matrix permeability. Comparing with the homogeneous case (Figure 4), we see that for large enough matrix permeabilities ($k_m \geq 10^{-5}$), the results are approximately the same and the fracture has little influence on the result.

From (4.1), we know that the effective permeability of the free-flow fracture of width $\ell = 0.01$ (assuming channel flow, i.e., no-slip boundary conditions at the sides of the fracture) is $k_f = \ell^2/12 \approx 10^{-5}$. Thus, we expect that at $k_m \approx 10^{-5}$, both the Darcy matrix permeability and the fracture permeability are of the same order. Indeed, in this range $k_{\text{eff}}/k_m \approx 1$. For $k_m << 10^{-5}$, the fracture has a significantly higher permeability than the surrounding matrix, and the effective permeability of the entire domain is larger than the matrix permeability, i.e., $k_{\text{eff}}/k_m > 1$.

If the matrix is in the Darcy regime ($k_m < 10^{-5}$), one can accurately reproduce the ef-

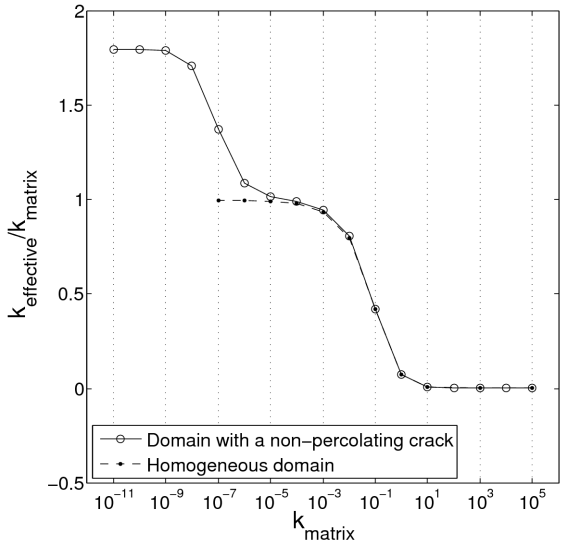

Figure 5: Computed effective permeability normalized by the matrix permeability for a square domain with a confined fracture of length 0.8 and width $\ell = 0.01$. In the matrix, Stokes–Brinkman equations are solved. Stokes equations alone are solved in the fracture. Results compared to the homogeneous case.

fective permeability computations for a confined free-flow fracture using a Darcy solver, and the Stokes–Brinkman solution is not necessary. Assuming k_f is described by (4.1) and $\ell = 0.01$, we set $k_f = \ell^2/12 \approx 10^{-5}$. Figure 6 shows a comparison of the effective permeability computed for various $k_m \leq k_f$ using a Darcy solver and corresponding computations based on the Stokes–Brinkman equations with a free-flow (Stokes) fracture. The results are in very good agreement.

It is possible to correctly reproduce the entire curve because of the assumptions made about the fracture permeability (4.1). In real-world scenarios—e.g., for the model presented in Section 2—one could argue that it is difficult to estimate k_f. Real fractures/channels have more complex shapes, and it may be difficult to obtain an adequate estimate of the fracture permeability. Thus, a Stokes–Brinkman computation could seem to be necessary. However, we note that this argument is only valid for small permeability ratios between the fracture and the matrix. For $k_m \leq 10^{-4} k_f$, which is the case in real scenarios (e.g., cm scale channels in a 1 mD matrix, [15]), the results saturate and the effective permeability is essentially governed by the matrix permeability. Regardless of the k_f value we use (as long as $k_m \leq 10^{-4} k_f$), the effective permeability is approximately the same.

We conclude that when a large-scale fracture is confined in a low permeability matrix, it is adequate to perform Darcy computations and set the fracture permeability anywhere around 4–5 orders of magnitude above the matrix permeability. This is illustrated in Table 1. Two examples are shown for k_m chosen so that the matrix is in the Darcy regime. We compute the effective permeability using the Darcy solver and set $k_f = 10^5 \cdot k_m$. The

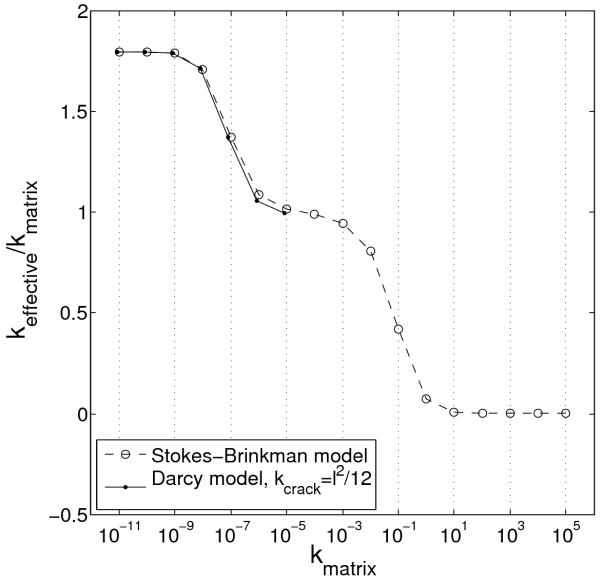

Figure 6: The plot shows computed effective permeability normalized by the matrix permeability for a square domain with confined fracture of length 0.8 and width $\ell = 0.01$. Darcy results (both fracture and matrix are pure Darcy domains) are compared to Stokes–Brinkman results. For the Darcy model, $k_f = \ell^2/12$.

Table 1: Comparison of Stokes–Brinkman and Darcy results. Fracture of length 0.8 and $\ell = 0.01$ confined in a low-permeable matrix. In the Darcy case, it is enough to set k_f to 4–5 orders of magnitude above the matrix permeability to obtain the same results, as in the case of a free-flow fracture.

	Darcy	Stokes–Brinkman	Darcy	Stokes–Brinkman
k_f	10^{-5}	∞	10^{-10}	∞
k_m	10^{-10}	10^{-10}	10^{-15}	10^{-15}
$\frac{k_{\text{eff}}}{k_m}$	1.80244	1.80245	1.80248	1.80273

results are compared to the Stokes–Brinkman solver with a free-flow fracture ($k_f = \infty$). The results for the Darcy and Stokes–Brinkman solvers are almost identical. Also, further decrease of the matrix permeability does not change the effect of the fracture on the effective permeability: k_{eff}/k_m is constant.

4.3 Through-Going Fracture

Another important scenario is that of a long-range channel/fracture. This case is modeled as a through-going rectangle connecting the left and right boundaries. In the case of a low-permeability matrix, the effective permeability of the entire domain is expected to be governed by the permeability of the free-flow (Stokes) domain.

Figure 7 shows a comparison of k_{eff} normalized by k_S, (4.1), for the two cases of a

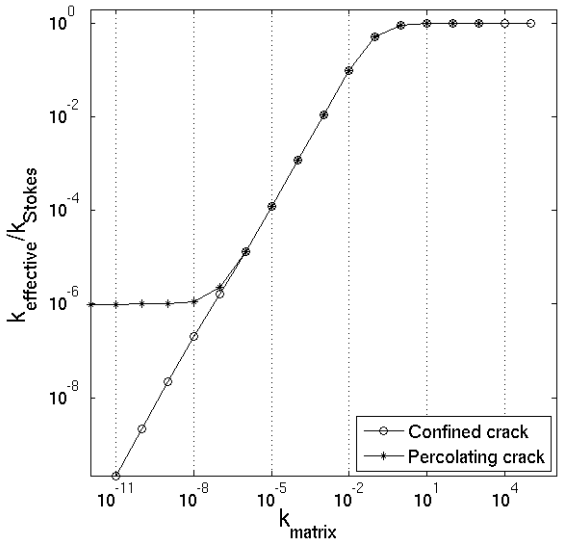

Figure 7: Square domain with a fracture of diameter $\ell = 0.01$. The plot shows the computed effective permeability. Results for through-going and confined fracture are compared. $k_f = \infty$ (free-flow Stokes domain).

through-going and a confined high-permeability fracture. For the through-going fracture with $k_m \ll k_f$, the effective permeability of the domain is constant and independent of k_m; that is, the velocities in the entire low-permeable matrix domain are negligible compared to the velocities in the fracture. In this case, the effective permeability given by (4.1) is modified by the volume fraction of the fracture:

$$k_{\text{eff}} = \frac{\ell^2}{12}\frac{\ell}{L}. \tag{4.3}$$

In the studied scenario, this means that

$$\frac{k_{\text{eff}}}{k_S} = \frac{0.01^3/12L}{L^2/12} = 10^{-6},$$

which is in agreement with the results from Figure 7.

It is clear from Figure 7 that for a through-going fracture with $k_f \approx 10^{-5}$ and $k_m \leq 10^{-9}$, the porous matrix does not contribute much, and the effective permeability of the entire domain can be obtained by a Stokes flow simulation.

5 Effective Permeabilities of a Carbonate Rock

In the previous section, we have shown that when a large difference in scales is observed in the setup, the use of Stokes–Brinkman equations is not necessary. All scenarios can then be then conveniently analyzed by the solvers dealing with the end-memeber cases.

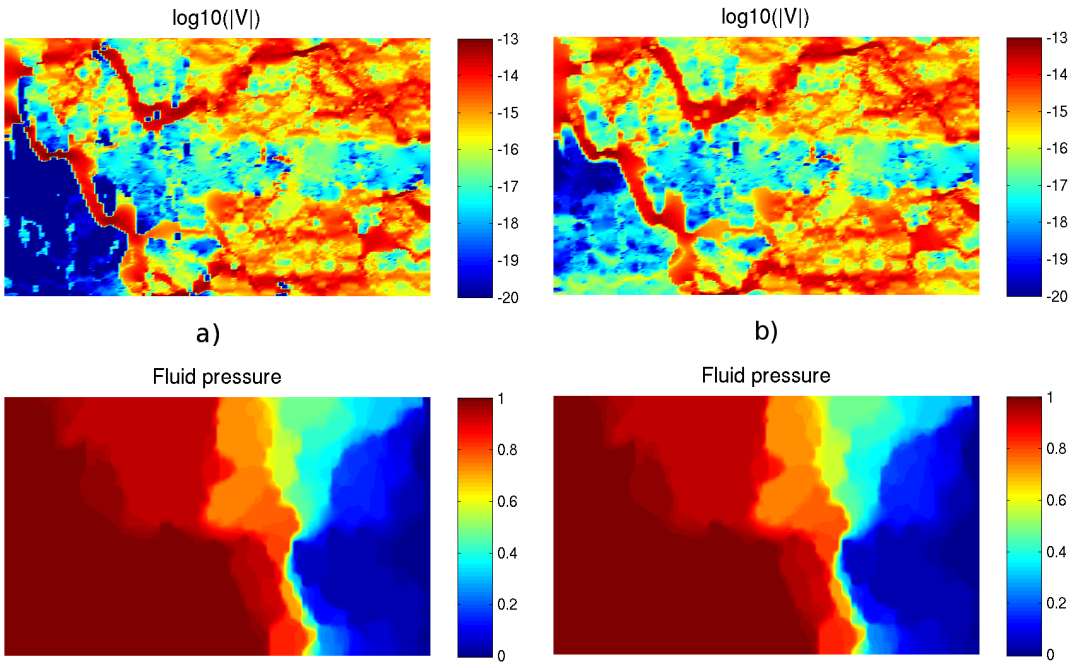

Figure 8: Velocity magnitude and pressure fields computed using the Stokes–Brinkman equations (left column) and the Darcy equations (right column) with pressure boundary conditions on left/right boundaries and free-slip on top/bottom boundaries. In the Stokes–Brinkman model, $k_f = \infty$ (pure Stokes). In the Darcy case, $k_f = 10 \max(k_m)$.

From the two-dimensional tests, we conclude that the required ratio of the permeabilities is $k_m / k_f \approx 10^{-4}$. The channel permeability can be accurately estimated from its diameter using (4.1).

Here, we compute the effective permeability of the real-world rock model presented in Section 2. In the following considerations, all the physical parameters are dimensional.

5.1 2D Cut

First, we analyze the effective permeability of a 2D cut through the 3D data, as shown in Figure 1. The vugs are not connecting the left and right sides of the model, which is analogous to the situation described in Section 4.2. We compute k_{eff} using both Stokes–Brinkman and a Darcy approach. In the Stokes–Brinkman case, we set $k_f = \infty$ (pure Stokes flow, no Darcy term). In the Darcy case, we set an arbitrary fracture permeability $k_f = 100$ mD, which is ten times the largest permeability found in the studied 2D section.

Computations took approximately 15 seconds on a desktop computer using the MILAMIN software. This includes building the matrix, factorizing the system, and visualizing the results.

Table 2: Effective permeability computed using Stokes–Brinkman equations (vugs are pure Stokes domains) and using Darcy equations. In the Darcy case, $k_f = 10 \max(k_m)$.

	Darcy	Stokes–Brinkman
k_f	100 mD	∞
k_{eff}	$7.44 \cdot 10^{-2}$ mD	$7.49 \cdot 10^{-2}$ mD

Figure 8 shows the computed fluid pressure and the magnitude of the velocity for both the Stokes–Brinkman and the Darcy simulations. The pressure fields are very similar for both cases:

$$\frac{\|p_D - p_{SB}\|}{\|p_{SB}\|} \approx 0.5\%$$

On the other hand, differences in the velocity fields can be seen by eye. This is not surprising, since the physics solved for in the vugs is very different. However, although locally the velocity fields may differ considerably for both methods, overall the flow patterns are similar.

Table 2 presents k_{eff} obtained using both methods. It is clear that, although the velocities may be different in both cases, this does not affect the computed effective permeability. The difference between k_{eff} in both cases is 0.7%. Thus, the Darcy solver can be used to compute the upscaled permeability values.

5.2 3D Model

The permeability field in Figure 1 is a 2D cut through the three-dimensional dataset. While the vugs/channels in all the 2D cuts are confined in the matrix, in three dimensions they do connect to the opposite sides of the domain, which illustrates the importance of 3D simulations. Figure 2 shows the channel structure in 3D.

The relevant idealized model is therefore the through-going fracture discussed in Section 4.3. The relatively impermeable matrix is not expected to significantly affect the effective permeability of this rock sample. Therefore, to compute k_{eff} we have removed the porous matrix from the model. The fact that we are able to do so is crucial from the point of view of the iterative solver. Large permeability ratios in the matrix, and the Stokes regime on a different spatial scale lead to a bad condition number that renders the original system very difficult to solve. On the other hand, by considering only the Stokes domain, we are dealing with channel flow of a homogeneous fluid—a task that is much simpler for an iterative method.

In the simulations, we apply ambient pressure gradient in the vertical direction. For the nodes lying on the channel boundary (marked in yellowish color in Figure 2), we set no-slip boundary condition. The mesh consists of around 800 000 cells (eight million nodes). It took 3 hours to solve the system on 360 Opteron cores of the Cray XT4 cluster.

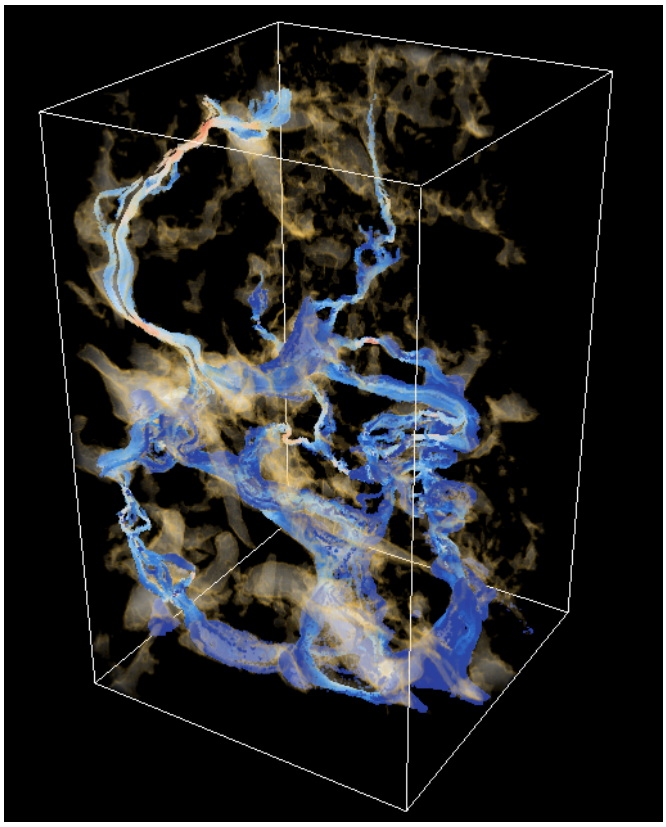

Figure 9: Stokes flow inside the fractures and vugs, without considering the porous matrix. Blue color of the streamlines denotes low velocity, red color marks high velocity. The model has 800 000 cells and eight million nodes.

Figure 9 shows the flow channels and fluid velocity through the vugs. For the purpose of visualization, we have placed half a million passive markers at $z=0$. The markers have been advected using the computed velocity field and a timestep chosen so that they are not transported further than to the neighbor cells. The markers are colored red in the high-velocity regions, and blue in the low-velocity regions. Some void spaces do not contain any markers—this indicates the stagnant zones. Clearly, studying the actual flow pattern is important if one wants to analyze e.g., the residual saturation. The effective permeability obtained from this calculation is $7.9 \cdot 10^5$ mD, i.e., much higher than the permeability of the surrounding porous matrix. This result further indicates that taking into account the Darcy matrix is not necessary in this case. As mentioned in Section 2, the highest permeability in the porous matrix is roughly 10^3 mD, while the average is much lower.

An estimate of how realistic the obtained effective permeability is, can be obtained as follows. As stated in Section 2, the spatial resolution of the CT scan is $0.5 \times 0.5 \times 1.5$ mm. Given that we are dealing with a percolating crack, we expect that the effective

permeability of the studied sample is at least that of a circular pipe with the diameter of a single grid cell. The 3D equivalent of equation (4.1) describing the effective permeability of a cylindrical pipe, based on the Hagen–Poiseuille equation, is

$$k_{pipe} = \frac{D^2}{32} \tag{5.1}$$

where D denotes the diameter or the pipe. Hence, the effective permeability of a non-permeable $13 \times 13 \times 21$ cm block with a through-going pipe of diameter 0.5mm, obtained by averaging k_{pipe} over the entire block surface, is 90 mD. On the other hand, a pipe of diameter 5 mm (ten times larger) yields an effective permeability of $9.0 \cdot 10^{-5}$ mD, which is on the same order as the computed result.

6 Concluding Remarks

In this paper, we have studied the effective permeability of a medium composed of long-range fractures and channels surrounded by a porous matrix with lower permeability. Our goal was to identify the parameters, for which the Stokes–Brinkman equations are applicable, and when the effective permeability can be computed by either Darcy or Stokes flow solvers alone. Being able to do so is advantageous from a numerical perspective, since the resulting systems of equations are better conditioned. We have considered three synthetic cases.

For a homogeneous two-dimensional channel of diameter L filled with an incompressible fluid and containing non-movable matrix with permeability k, we have shown that the Stokes flow is dominant for $k/L^2 \geq 10$. For $k/L^2 \leq 10^{-4}$, an accurate effective permeability can be obtained by a Darcy flow solver. For $10^{-4} \leq k/L^2 \leq 10$, the Stokes–Brinkman equations should be used to account for the transition between the end-member flow regimes.

The effective permeability of a domain with a large, non-percolating, free-flow crack confined within a low permeability matrix can be computed using a Darcy flow solver. The actual permeability of the fracture is not relevant and can be set to an arbitrary value such that $k_f \geq 10^4 k_m$. Further increase in the fracture permeability does not change the computed effective permeability.

The effective permeability of a domain with a large, through-going, free-flow fracture surrounded by a low permeability matrix can be computed using a Stokes flow solver. When $k_f \geq 10^4 k_m$, the velocities in the Darcy matrix are negligible and do not significantly contribute to the effective permeability.

For the systems studied, we have shown that to compute the effective permeability, the Stokes–Brinkman equations are applicable only when the ratio between the crack and matrix permeability does not exceed 4 orders of magnitude. Otherwise, Darcy or Stokes solvers can be used. These findings have been verified for 2D models obtained from a CT scan of a rock sample.

A quick determination of the importance of the Stokes–Brinkman equations can be performed by estimating the effective vug permeability of natural rocks with (5.1). Only if this permeability is within the four orders of magnitude from the matrix permeability must the Stokes–Brinkman equations be considered. For natural systems, this is only the case for very narrow (typically sub millimeter) vugs.

Our findings allow for effective permeability computations directly on CT rock sample data, which would otherwise be not feasible. We demonstrate this with the case of a carbonate rock sample. Based on our analysis, we identified Stokes flow as the appropriate model and successfully computed the effective permeability on a 3D model containing 8 million cells. Other approaches that try to reduce the computational cost, such as 2D models or two-step upscaling, fail to give an accurate permeability estimate because they cannot account for the effect of percolating cracks.

Acknowledgments

This study has mostly been performed using computational facilities provided by the Norwegian Metacenter for Computational Science (NOTUR). The work of Krotkiewski and Schmid was supported by a Center of Excellence grant from the Norwegian Research Council to PGP (Physics of Geological Processes) at the University of Oslo. The authors would like to thank Marcin Dabrowski for insightful discussions.

The research of Ligaarden and Lie was funded in part by Shell Norge AS and the Research Council of Norway through grants no. 175962 and 186935. Lie also acknowledges partial funding from the Center of Mathematics for Applications, University of Oslo.

The Pipe Creek CT-scan data was originally collected by the Bureau of Economic Geology at The University of Texas at Austin with funding from the Industrial Associates of the Reservoir Characterization Research Laboratory. The authors are grateful to Bob Loucks, Chris Zahm, and Jim Jennings for assistance in accessing the data.

References

[1] T. Arbogast and D. S. Brunson. A computational method for approximating a Darcy–Stokes system governing a vuggy porous medium. *Comput. Geosci.*, 11(3):207–218, 2007.

[2] T. Arbogast and M. S. M. Gomez. A discretization and multigrid solver for a Darcy–Stokes system of three dimensional vuggy porous media. *Comput. Geosci.*, 2009. Doi: 10.1007/s10596-008-9121-y.

[3] T. Arbogast and H. L. Lehr. Homogenization of a Darcy–Stokes system modeling vuggy porous media. *Comput. Geosci.*, 10(3):291–302, 2006.

[4] G. S. Beavers and D. D. Joseph. Boundary conditions at a naturally permeable wall. *Journal of Fluid Mechanics*, 30:197–207, 1967.

[5] H. C. Brinkman. A calculation of the viscous force exerted by a flowing fluid on a dense swarm of particles. *Applied Scientific Research Section a-Mechanics Heat Chemical Engineering Mathematical Methods*, 1(1):27–34, 1947.

[6] M. Dabrowski, M. Krotkiewski, and D. W. Schmid. MILAMIN: MATLAB-based finite element method solver for large problems. *Geochem. Geophys. Geosyst.*, 9(1), 2008.

[7] T. A. Davis and W. W. Hager. Row modifications of a sparse Cholesky factorization. *Siam Journal on Matrix Analysis and Applications*, 26(3):621–639, 2005.

[8] H. Elman, D. Silvester, and A. Wathen. *Finite Elements and Fast Iterative Solvers (with Applications in Incompressible Fluid Dynamics)*. Numerical Mathematics and Scientific Computation. Oxford University Press, 2005.

[9] A. F. Gulbransen, V. L. Hauge, and K.-A. Lie. A multiscale mixed finite element method for vuggy and naturally fractured reservoirs. *SPE J.*, 15(2), 2010.

[10] J. W. Jennings and F. J. Lucia. Predicting permeability from well logs in carbonates with a link to geology for interwell permeability mapping. *SPE Reservoir Evaluation & Engineering*, 6(4):215–225, 2003.

[11] T. Karper, K.-A. Mardal, and R. Winther. Unified finite element discretizations of coupled Darcy–Stokes flow. *Numer. Meth. PDEs*, 25(2):311–326, 2009. Doi: 10.1002/num.20349.

[12] M. Krotkiewski and M. Dabrowski. Parallel symmetric sparse matrix-vector product on scalar multi-core cpus. *Parallel Computing*, 36(4):181 – 198, 2010.

[13] S. Liu and J. H. Masliyah. Dispersion in porous media. In K. Vafai, editor, *Handbook of porous media*, page 110. CRC Press, 2nd edition, 2005.

[14] P. Popov, Y. Efendiev, and G. Qin. Multiscale modeling and simulations of flows in naturally fractured karst reservoirs. *Commun. Comput. Phys.*, 6:162–184, 2009.

[15] P. Popov, G. Qin, L. Bi, Y. Efendiev, Z. Kang, and J. Li. Multiphysics and multiscale methods for modeling fluid flow through naturally fractured carbonate karst reservoirs. *SPE Reservoir Evaluation & Engineering*, 12(2):218–231, 2009.

[16] P. Renard and G. de Marsily. Calculating equivalent permeability: A review. *Advances in Water Resources*, 20(5–6):253–278, 1997.

[17] J. Shewchuk. Triangle mesh generator, 2007. `http://www.cs.cmu.edu/ quake/triangle.html`.

[18] J. Willems. *Numerical Upscaling for Multiscale Flow Problems*. PhD thesis, Technische Universität Kaiserslautern, 2009.

[19] L. Zhang, S. L. Bryant, J. W. Jennings, T. J. Arbogast, and R. Paruchuri. Multiscale flow and transport in highly heterogeneous carbonates. In *Proceedings of the SPE Annual Technical Conference and Exhibition*, September 2004. SPE 90336.